Deep Mining 2024 – P Andrieux & D Cumming-Potvin (eds)

doi:10.36487/ACG_repo/2465_78

Effects of yielding pillars and chevron sequences on convergence and released energy in sublevel cave mining

Joel Andersson [a,*], Jonny Sjöberg [a], Mikael Svartsjaern [a], Jimmy Töyrä [b], Matthias Wimmer [b], Graham Swan [c]

[a] *ITASCA, Sweden*

[b] *LKAB, Sweden*

[c] *HeadMining AB, Sweden*

Abstract

Yielding pillars have been effectively employed in many underground hard rock mines as a means of support, with pillars designed to yield in a ductile manner to mitigate rockbursts. The concept has so far mainly been applied to cut-and-fill and blasthole stoping with consolidated backfill mining methods. For sublevel cave mining in the LKAB Kiirunavaara Mine, the hanging wall–footwall convergence, over the length of the orebody, is one potential factor that can contribute to release of energy associated with seismic events. By implementing a configuration with large-scale yielding ore pillars, it is theorised that the rate of convergence per mined volume can be reduced, thus also reducing the seismic potential in the mine. To assess the feasibility of this approach, a 3D numerical model was utilised to analyse convergence and energy release effects. The study aimed to demonstrate conceptually, but with a representative orebody geometry, that the proposed mining concept with yielding pillars and a chevron sequence can result in reduced convergence and/or released energy. Four mining scenarios were evaluated, including standard sublevel caving and an alternative chevron-shaped mining front, with and without yielding pillars included. The results suggest that employing yielding pillars could effectively mitigate seismic potential by reducing convergence rates and energy release. However, the specifics of pillar design, including size and recovery, require further investigation. This research and development work contributes to ongoing efforts to improve safety and efficiency in underground mining operations in the LKAB Kiirunavaara Mine.

Keywords: *sublevel caving, numerical modelling, mine seismicity, pillars*

1 Introduction

1.1 Background

The concept of yielding pillars has been successfully applied as a means of support in many underground hard rock mines, mainly for cut-and-fill and/or sublevel stoping mining methods (e.g. du Plessis 2018). Yielding pillars mobilise a large-scale reinforcement effect through providing a stable volume maintaining a lower residual strength. Hence the pillars are designed to not fail violently but instead in a ductile manner, thus alleviating the potential for associated rockbursts.

Yielding pillars could also be expected to control the convergence between the hanging wall and footwall when mining, even for other mining methods. A case in point is the LKAB Kiirunavaara Mine in northern Sweden, where iron ore is mined underground using sublevel caving. Extensive mining-induced seismicity has been recorded since 2008 (Dahnér et al. 2012). The hanging wall–footwall convergence, over the length of the 4,000 m-long orebody, is one potential factor that can contribute to the release of energy associated with seismic events. By designing a mining configuration with large-scale yielding pillars, it is believed that

* Corresponding author. Email address: joel@itasca.se

the rate of convergence per mined volume can be reduced, thus also reducing the seismic potential in the mine with deeper mining.

The concept of yielding pillars has been used with some success in deep Canadian mines and would potentially serve to reduce the rate of convergence per tonne of ore mined on a given level. With fairly large variations in geology and geometry along the Kiirunavaara orebody, spontaneous and unconstrained failures causing unpredictable convergence-driven seismicity are expected. A measure of constraint on convergence would be provided by leaving ore pillars that yield. To investigate the applicability of a yielding pillar layout for the Kiirunavaara Mine, a 3D numerical model was used to study the effects on convergence and energy release, following in part the approach used by Mortazavi & Brummer (2000) but in 3D and with multiple pillars.

1.2 Objective, scope and approach

The overall aim of the study was to demonstrate conceptually, but with a representative orebody geometry, that the proposed mining concept can result in reduced rates of convergence and released energy. The yielding pillars should also maintain some load-bearing capacity throughout the mining process. However, a more detailed design study, including fine-tuning of the mining layout, pillar size, recovery of pillars, etc. was outside the scope of this initial study.

The work comprised 3D numerical modelling of the LKAB Kiirunavaara Mine using a mine-scale model. The rock mass was simulated as a strain softening material, with representative properties for the host rock and ore based on existing test data and existing experience within LKAB and ITASCA. To this purpose, the *IMASS* (Itasca Constitutive Model for Advance Strain Softening) material model (Ghazvinian et al. 2020) was used. All analyses were conducted using the *FLAC3D* finite difference code (ITASCA 2022). The numerical model was run for a set of cases with alternative mining sequences, and with and without pillars included. The results were primarily evaluated with respect to convergence, plastic state and released energy, with comparisons made between the different cases.

2 Methodology

2.1 Mining scenarios

Both the applied mining sequence and the inclusion of pillars will affect convergence and released energy. An alternative, and possibly more optimal, mining sequence was studied in addition to the currently planned (flat) sublevel cave sequence. A chevron-shaped mining front is often employed in, for example, sublevel stoping mines and gives good results; thus a similar mining front was developed and analysed for comparison with the base case (sublevel caving) sequence. The two sequences were analysed, without and with a pillar layout, to quantify the separate effects of the mining sequence. Hence the following four cases were run:

1. base case – standard sublevel caving with mining to the 1,365 m level (current main haulage level)
2. chevron case – alternative mining sequence with a chevron geometry of the mining front, with mining to the 1,365 m level
3. base case with pillars – same sequence as in the base case but with pillars included
4. chevron case with pillars – same chevron sequence but with pillars included.

Models are run for historic mining until 2020 for the base case (i.e. prior to the large seismic event in the mine, e.g. Svartsjaern et al. [2022]) to enable comparisons with observed behaviour. For the chevron sequence, mining was conducted until an ‘equivalent year’ of 2017 (further described below). For future mining the models were run for mining down to the 1,365 m level.

2.2 Quantifying the potential energy release

Energy balance, or the release of it, in the numerical model was studied using the concepts described by Hedley (1992) and Ortlepp (1983). The theory is based on linear elastic response but is assumed to be, at least in parts, also applicable to plastic material behaviour. The energy balance equation is formulated as follows:

$$Wt + Um = Uc + Ws + Wr \quad (1)$$

where:

W_t = change in potential energy (work)

U_m = stored (strain) energy in removed rock volume

U_c = stored (strain) energy in remaining rock

W_s = absorbed energy in backfill (caved rock) and support

W_r = released energy.

The change in potential energy can be calculated as the product of the volumetric convergence, V_c, and the stress acting in the direction of convergence, σ_{11}, i.e.:

$$W_t = \sigma_{11} \times V_c \quad (2)$$

The strain energy in the removed rock and the remaining rock can be calculated as:

$$U_m = \Sigma_{removed}\Delta(\sigma_{ij}\varepsilon_{ij}) \quad (3)$$

$$U_c = \Sigma_{remaining}\Delta(\sigma_{ij}\varepsilon_{ij}) \quad (4)$$

where:

$\Delta(\sigma_{ij}\varepsilon_{ij})$ = the sum of the strain energy (product of stress and strain for all stress/strain tensor components) in the removed and remaining rock, respectively.

Similarly, the energy absorbed by the caved rock can be calculated as:

$$W_m = \Sigma_{caved\ rock}\Delta(\sigma_{ij}\varepsilon_{ij}) \quad (5)$$

By rearranging Equation 1 and using Equations 2, 3, 4 and 5, the released energy can be calculated as follows:

$$W_r = \sigma_{11} \times V_c + \Sigma_{removed}\Delta(\sigma_{ij}\varepsilon_{ij}) - \Sigma_{remaining}\Delta(\sigma_{ij}\varepsilon_{ij}) - \Sigma_{caved\ rock}\Delta(\sigma_{ij}\varepsilon_{ij}) \quad (6)$$

All components are retrieved directly from the numerical model for each element in the caved rock, the removed rock and the remaining rock, respectively. The released energy, W_r, is assumed to be related to seismic energy (in some proportion) and is thus used to compare the different cases with respect to 'seismic potential'. Energy is normalised with respect to extracted tonnage to enable relevant comparisons between different cases and mining stages. The above equations were originally based on the theory of elasticity. The fact that there is yielding in the rock material may have some influence on their validity although the overall concept is still applicable.

3 Numerical model

3.1 Geology

The main geological model consists of the orebody boundary (ore), two diabase dykes (DB), clay alterations (clay), porphyry dykes (QP) and the host rock (varying types of trachyandesite or syenite and quartz porphyries), which are shown in Figure 1. The orebody varies significantly in thickness, from virtually 0 m to approximately 210 m. The rock mass was modelled using the *IMASS*; see Ghazvinian et al. 2020) with properties according to Table 1. These properties were based on previously calibrated numerical models for

the Kiirunavaara Mine. To inhibit excessive deformation of the hanging wall caused by the caving process, the hanging wall was modelled as an 'equivalent-elastic' material with a high UCS value (σ_{ci} = 1,000 MPa).

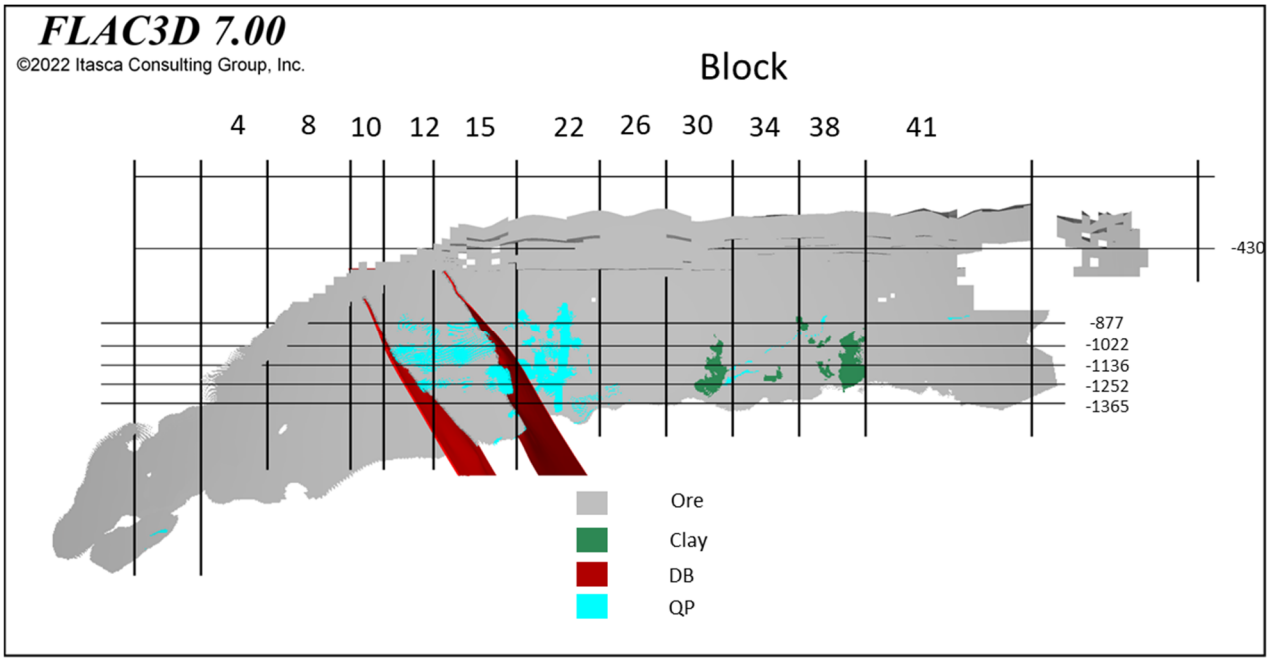

Figure 1 Geological units in the model

Table 1 Rock mass properties for the main geological units

Property	Footwall	Hanging wall	Ore	Diabase (DB)	Quartz porphyry (QP)	Clay zones*
Density (kg/m^3)	2,800	2,800	4,600	2,800	2,800	2,000
Intact Young's modulus (GPa)	62	66	93	65	65	0.01
UCSi (MPa)	180	1,000	133	175	320	–
GSI	76	66	67	44	81	–
mi	20	18	17	15	20	–
Residual friction angle (°)	30	30	30	30	30	3.5**
Dilation angle (°)	10	10	10	10	10	10

*Clay zones are modelled using a perfectly plastic Mohr–Coulomb material model. **Internal friction angle

3.2 Geometry

A mine-scale numerical model of the entire Kiirunavaara Mine was set up to simulate sublevel cave mining. The model was built with *FLAC3D* (ITASCA 2022) using an 'octree' or 'sugar cube' shaped mesh with model dimensions of 4,500 × 7,000 m and a depth of 2,500 m. The elements in the model vary in size from 6.25 m side lengths in areas of interest to 100 m side lengths at the model boundaries. Initial stresses were based on the compilation by Sandström (2023). Roller boundaries were used on the vertical sides as well as the bottom side of the model, with the ground surface modelled as a free surface boundary.

Four explicit slip planes were also included in the model, simulating the weak contact on each side of the two diabase dykes. These slip planes were included as explicit interfaces located in two local tetrahedron meshes (one for each diabase dyke) attached to the global octree mesh.

3.3 Mining sequences

3.3.1 Base case sequence

Historic mining from the surface to the year 1996 was simplified and conducted in the same way for all four cases, in accordance with Figure 2. Mining in the model was performed by mining the entire level in one production block during the year when that level and production block was disconnected from the hanging wall (see Figure 2 for an example). The mining process is simulated by assigning an initial zero stress state in the portion of the orebody flagged for mining during that step by changing the material model from *IMASS* to a Mohr–Coulomb material for caved rock, with an intermittent 'null' step.

Mining with the base case sequence up to 2020 was based on historic data, while mining from 2021 forward was based on the mining plan delivered by LKAB to ITASCA. As a result of the 2020 seismic event in the mine, an area in production block 22 was not mined due to damages on levels 1,022 and 1,052 m. This volume was also left unmined in the base case sequence. However, these levels are mined for the chevron sequence.

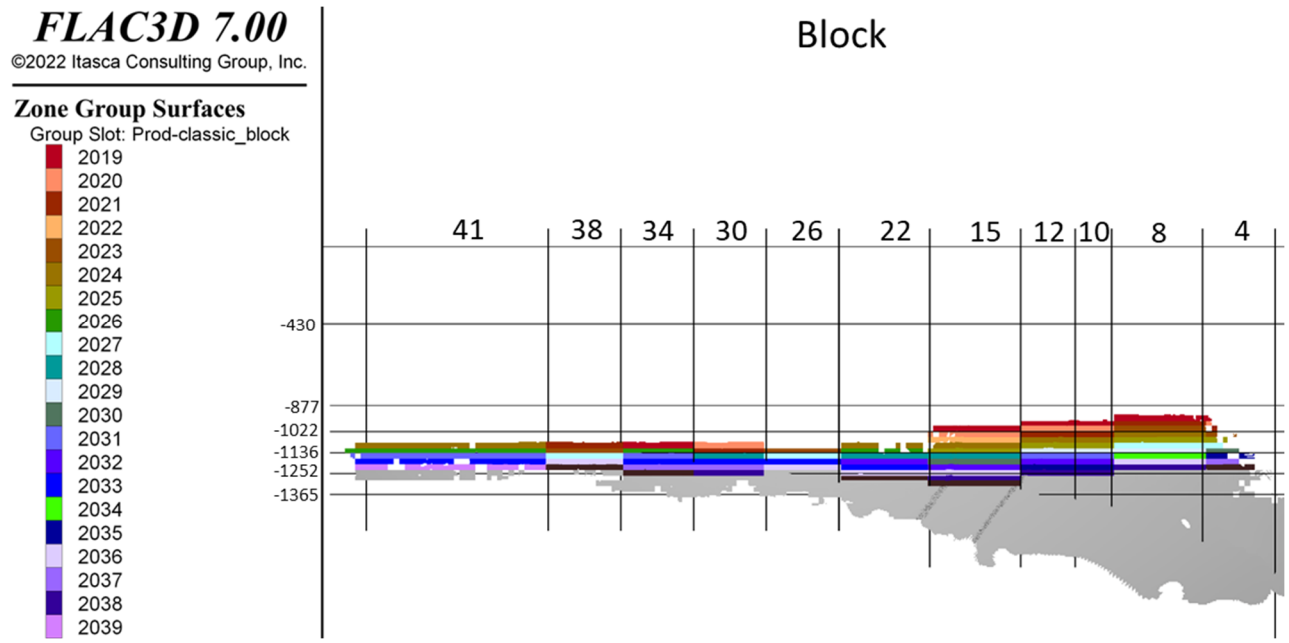

Figure 2 Base case sequence for the years 2019–2040

3.3.2 Chevron case sequence

The chevron sequence starts with a single 200 m-wide chevron tip placed in the centre of block 22 on level 740 m. After four years of mining, the chevron shape has been established in the model with a chevron angle of approximately 20°. The volume mined from the model using the chevron sequence each year was the same as the volume in the base case. Production years for the chevron case is noted as 'equivalent year' for historic and future mining steps since it is a fictional scenario simulating how mining would have progressed should it have been conducted using a chevron-shaped mining sequence from 1997 rather than the actual historic mining. The chevron sequence was mined down to the 1,365 m level in production block 22 (Figure 3a).

When the tip of the chevron in production block 22 has reached the 1,365 m level the mining sequence continues with two chevrons on either side. The chevron tip for the southern chevron was placed in production block 34 and the tip of the northern chevron was placed in production block 8. These two chevrons were mined with the same chevron angle and tip width as the initial chevron in production block 22. Mining with two chevron fronts was continued until the two chevron tips reached the 1,365 m level, at the equivalent year 2038 (Figure 3b).

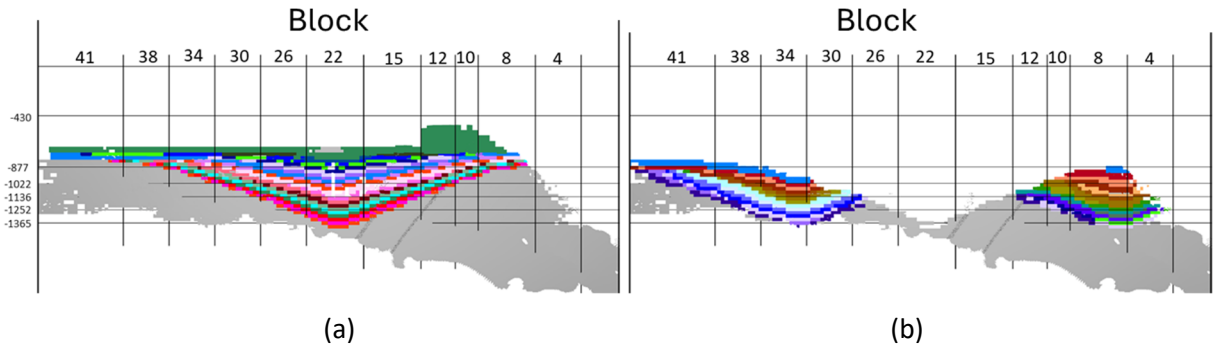

Figure 3 Chevron sequence for the equivalent years of: (a) 1997–2017; (b) 2018–2038

3.3.3 Mining sequence for pillar cases

The only difference in the mining sequence between the models that have yielding pillars compared to the model with no yielding pillars was that ore located in the pillars was left unmined. The overall sequence remains the same; hence, the volume mined per 'year' is slightly less in the case with pillars.

3.3.4 Yielding pillar layout

The yielding pillars were designed as continuous, vertical (rib) pillars extending from approximately the 700 m level to the 1,365 m level. The initial pillar is placed in the centre of block 22, with the following pillars placed along the orebody at different spacings depending on the thickness of the orebody. The final pillar dimensions were reached iteratively, as follows:

- The first design was based on 'back of the envelope' empirical calculations and the average ore thickness for each production block. Calculations used a target width:height (width in the ore strike direction:height of the orebody thickness) and width:stope span (where stope span is along the orebody strike) of 0.75 and 0.31, respectively. This pillar configuration was evaluated using the numerical model and initial results showed limited yielding of the pillars.
- Design modifications were implemented to increase yielding in the pillars. The width of all pillars (in the ore strike direction) was decreased and set to 60 m, and some pillars were removed. This resulted in acceptable yielding in the pillars (with one notable exception, to be described further below). The extraction ratio using this pillar configuration is 81%.

It is important to note that the selected pillar layout is not optimised. The goal of this pillar layout was to have a working yielding pillar design that reasonably fit the orebody. The design has the potential to be improved from rock mechanics, operational and economic standpoints as well as ensuring that yielding of the pillars develops in a ductile manner.

4 Released energy

4.1 Comparison of base case and chevron case

Since the mining sequences of the base case and the chevron case are different it would be incorrect to compare them for the same year. The two cases are instead compared at stages when the mining front in block 22 is at the same mining level. Mining using the chevron sequence has the production spread over a larger portion of the orebody in comparison to the base case. For the base case, the whole production block is always mined. In the chevron case, portions of a production block may be mined, which tends to result in the mining being concentrated on a smaller area for each year. The chevron case results in released energy in more production blocks (Figures 4 and 5) but the peak values of released energy are reduced compared to the base case. All energy quantities are normalised with respect to the extracted volume for each period and each production block.

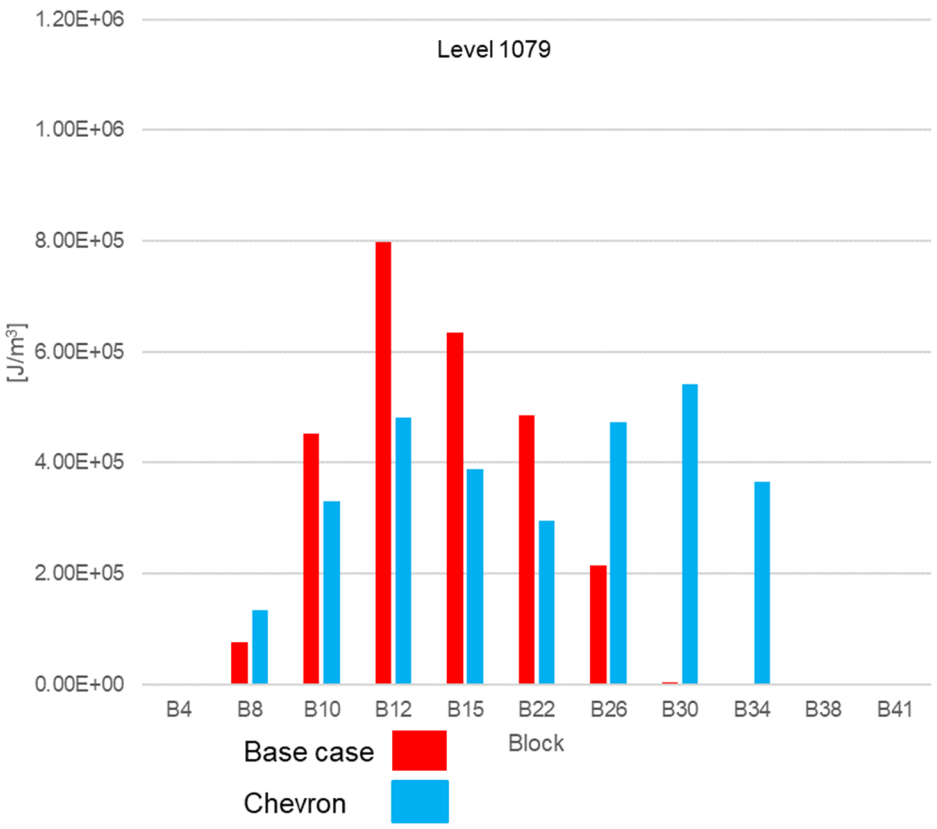

Figure 4 Released energy in each mining block when mining has started at the 1,079 m level

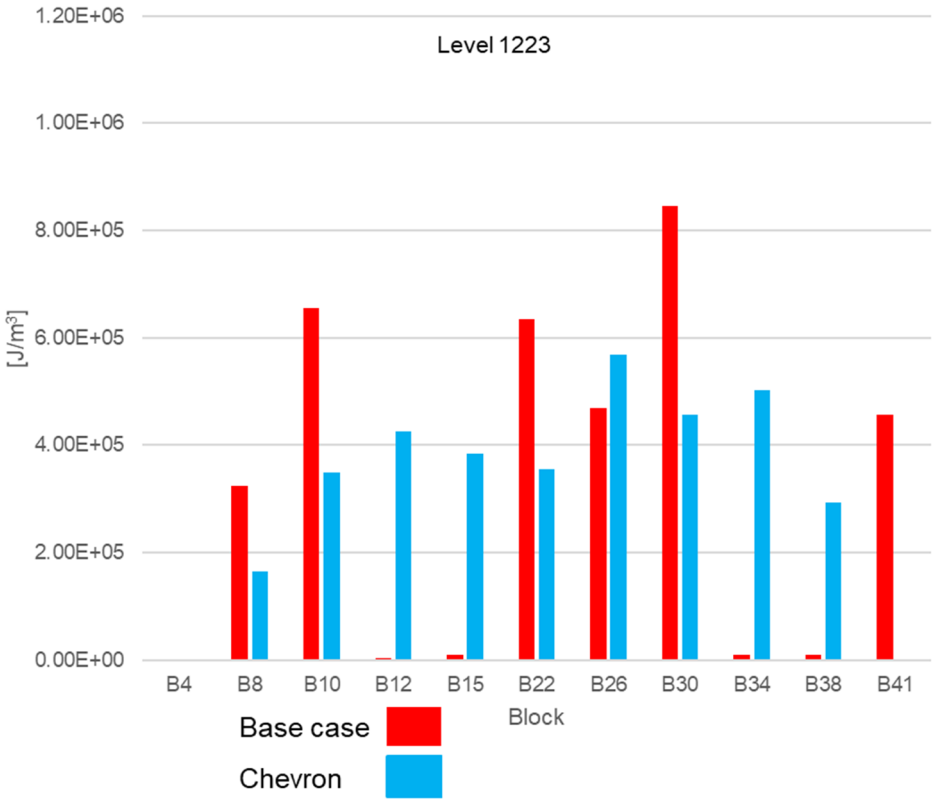

Figure 5 Released energy in each mining block when mining has started at the 1,223 m level

It can also be noted that, at least for the base case, the peak energy value increases with depth, which can probably be explained by the increased stress magnitude that follows with increasing depth. A comparison of the cumulative released energy versus the cumulative volume of ore mined in the model is shown in Figure 6. The chevron sequence generates a lower amount of released energy for the same volume of ore mined compared to the base case. After the first chevron is completed, a slight change can be observed in which the difference in released energy between the two cases increases more. One explanation for this could be that the two unmined areas between the chevron fronts act as barrier pillars, thus reducing the overall convergence. A secondary effect may be that the tip of the chevron mining front is located at shallower depths compared to the base case and hence in a more favourable (lower) stress environment.

The chevron sequence has a lower cumulative released energy than the base case for the same amount of ore mined during the entire sequence. This indicates that there is potential to reduce released energy by changes in the mining sequence. The analysed chevron sequence stops at the 1,365 m level, which means that there are portions of the orebody left unmined in comparison to the base case. There is a possibility that if the remining areas are mined, the cumulative energy for the chevron case will catch up to the base case. However, given that the inclination of the curve for the chevron case remains lower than that for the base case, it does have a reduced rate of energy release during the entire sequence; it is possible that it would continue to do so until the same amount of ore was mined.

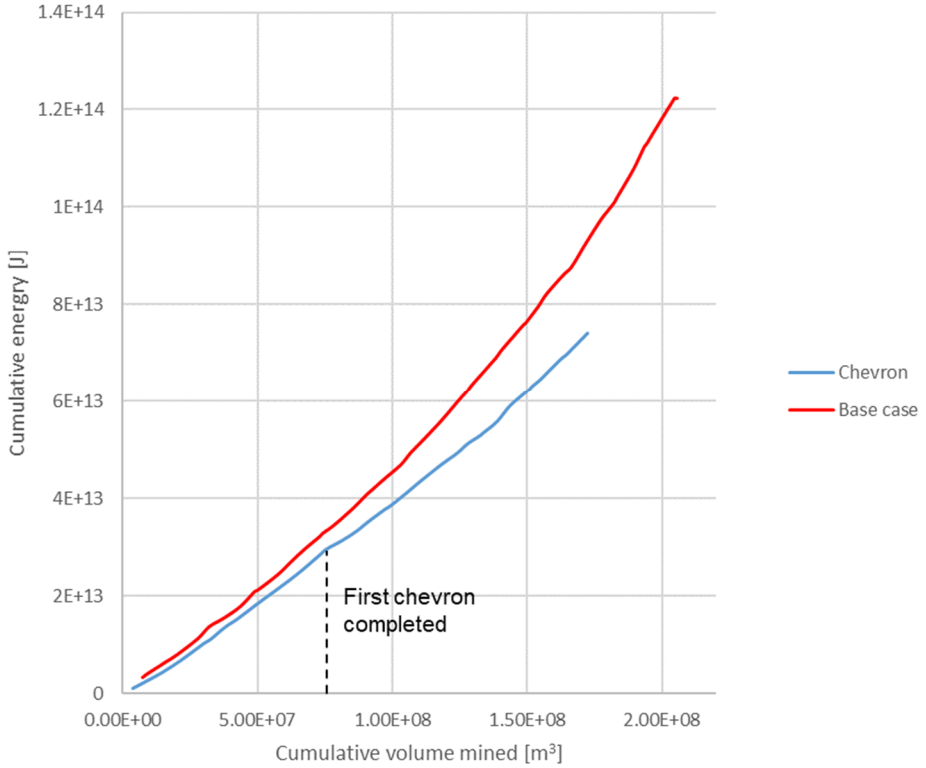

Figure 6 Cumulative released energy versus cumulative mined volume for the base and chevron cases

4.2 Pillar versus non-pillar cases

Mining using both the base case and chevron case was also simulated with yielding pillars. With the pillars included, the results indicate that in all the production blocks where energy is released for both historic and future mining years, the released energy is lower in the yielding pillar model compared to the non-pillar model (Figures 7 and 8). The pattern for how the released energy is distributed between the different production blocks for each year is similar to the case with yielding pillars and the non-pillar case. This could indicate a similar behaviour in energy release between the two cases, with a reduction in energy magnitude from the inclusion of yielding pillars in the mining layout.

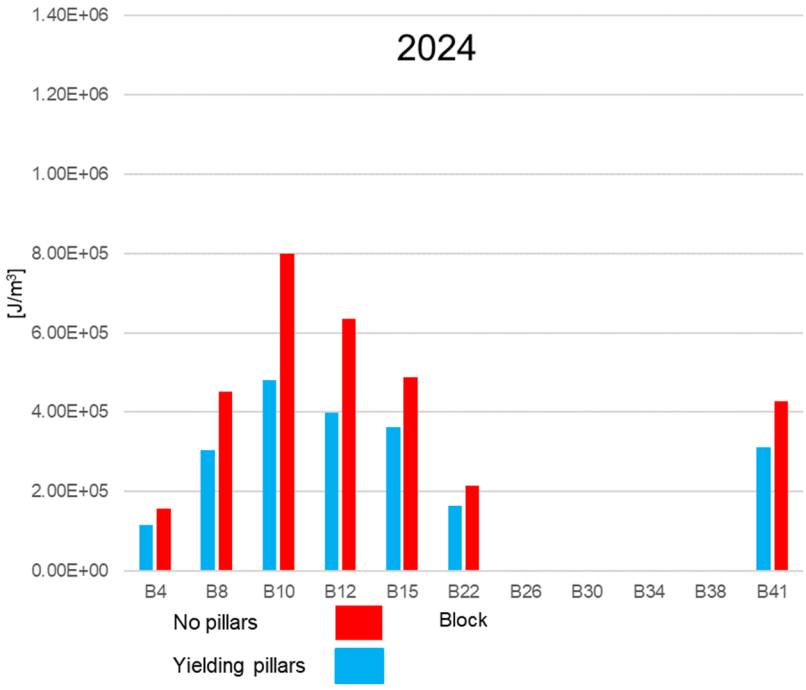

Figure 7 Released energy for the base case with and without yielding pillars for production in the year 2024

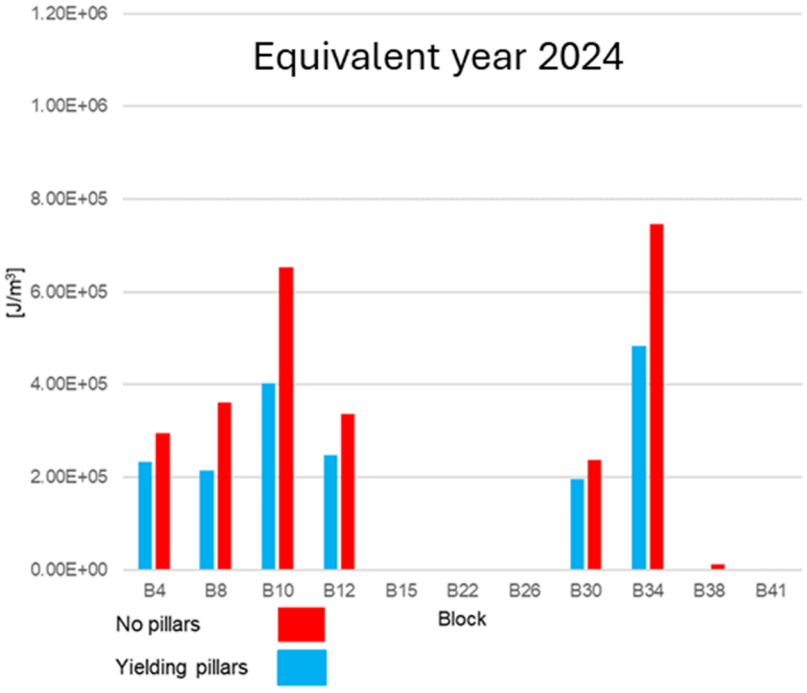

Figure 8 Released energy for the chevron case with and without yielding pillars for production in the equivalent year 2024

Looking at the cumulative released energy for all four cases in Figure 9, the usage of yielding pillars reduces the released energy for both the base case and the chevron case in comparison to the same model without yielding pillars. For the base case, the reduction in released energy for the model with yielding pillars is decreasing towards the end of the sequence. This trend is not seen when comparing the yielding pillar and non-pillar cases for the chevron sequence.

This difference may be due to the base case being mined with a larger portion of its mining front located at greater depths compared to the chevron sequence, in particular towards the end of the sequence, thus resulting in an increase in stress. The chevron sequence would likely show a similar behaviour eventually if more of the orebody was mined with that sequence. This can be simulated by continuing the chevron sequence with the chevron tips going below the 1,365 m level. Based on these results it is probable that the largest reduction in released energy can be achieved by first implementing a chevron and then by using yielding pillars.

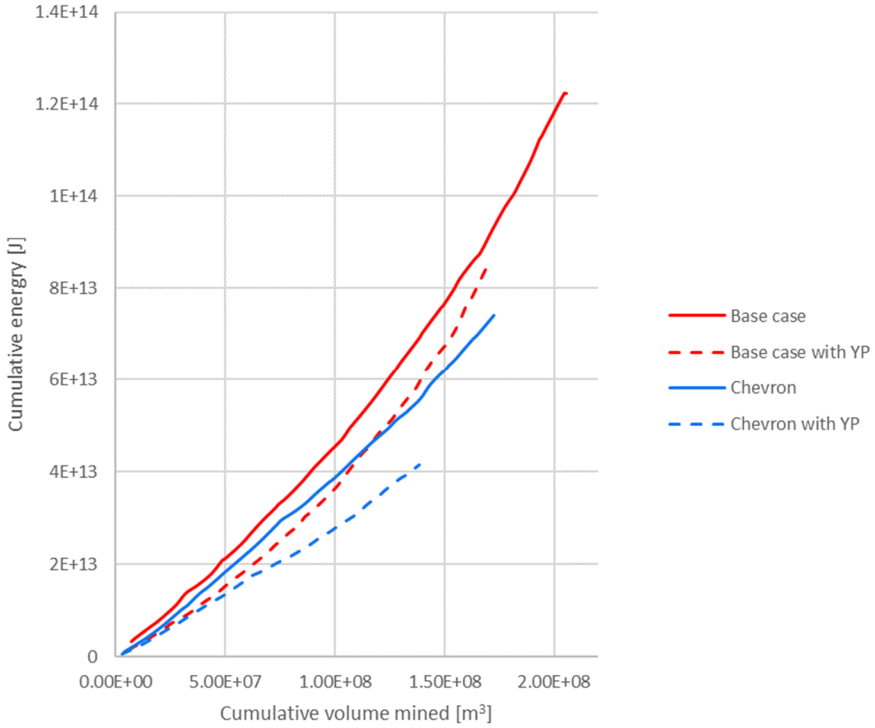

Figure 9 Cumulative energy versus cumulative volume mined for all four cases

4.3 Comparison with observations

Historic mining simulated in the base case can be compared with recorded seismic activity. This was done to see if correlations can be made between the released energy from the model and observed historic seismic events. Seismic events larger than ML > 1 for the period 2008–2022 were separated into events that occurred in the footwall and those occurring in the orebody. Hanging wall events were excluded because this was not an area of interest and localisation errors are larger on the hanging wall side (due to ray paths having to go around the caved areas). The location of the filtered events was visualised together with the released energy calculated from the numerical model, using the base case in each production block for the corresponding year.

Comparison of the location of seismic events versus the location and amount of released energy showed some qualitative agreement both for events occurring in the orebody as well as for events in the footwall (Figure 10). However, for many compared years the released energy correlates poorly with the location of the seismic events (as exemplified in Figure 11).

The fact that seismic events do not seem to always align with concentrations of released energy, however, does not necessarily mean that there is a poor correlation. If the entire mining area is considered as one mechanical system, the weakest point in that system will be the one reacting to the released energy. If, for example, there is weak structure far away from the point of energy release, but all more nearby structures are stronger, then a seismic event may occur far away from the point of maximum energy release.

The calculation of released energy is tied, to a large proportion, to where mining in the model is conducted and thus not necessarily where, for example, fault slip events have occurred. Hence to achieve a larger

accuracy and possible better comparison with observations, a more detailed mining sequence and/or a different way of calculation energy from the model would be needed. Also it may be worthwhile to compare seismic energy levels independent of event location.

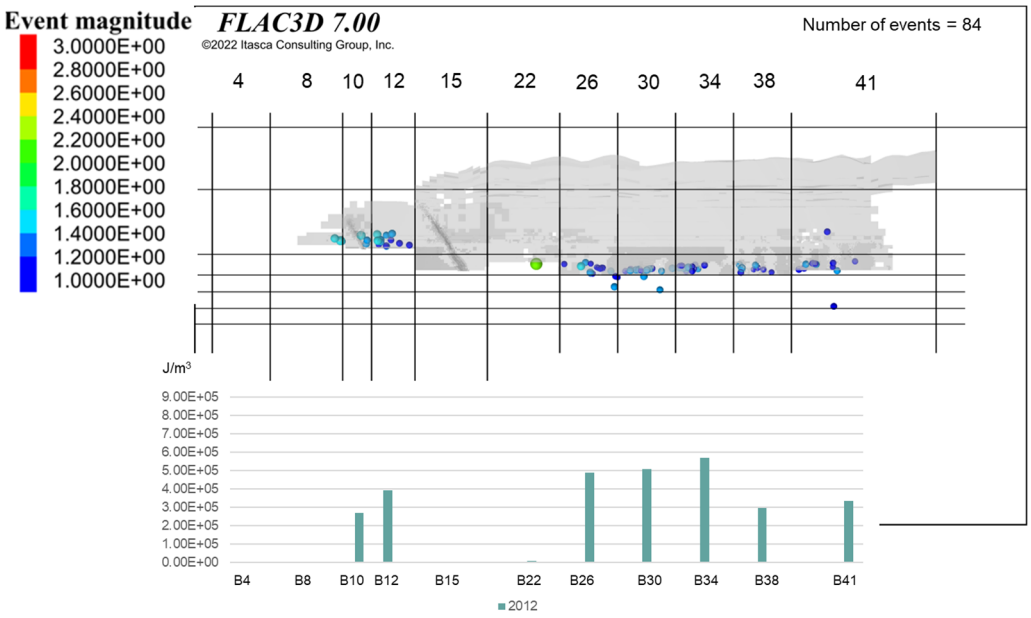

Figure 10 Footwall events for 2012. The greyed-out area shows the progression of the mining front

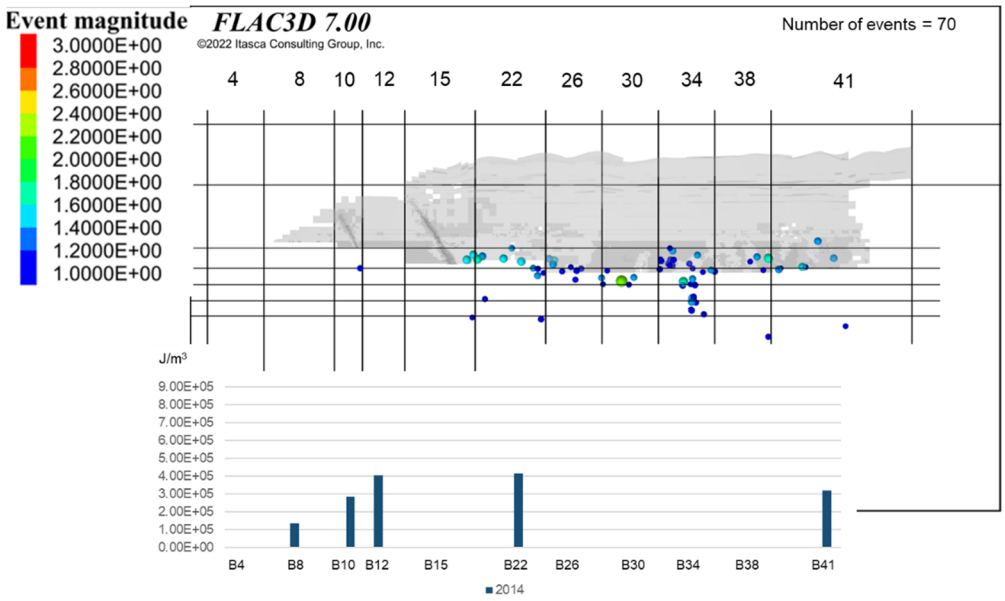

Figure 11 Footwall events for 2014. The greyed-out area shows the progression of the mining front

5 Pillar behaviour

Pillars were introduced in the sequence to reduce the convergence. Ideally the pillars should yield in a ductile way to prevent violent failures. The potential for ductile failure cannot be evaluated using the current model, however, the pillar stresses and the load-shedding were studied as follows.

An overview of the yielding in the pillars together with the mined rock is shown in Figure 12. Similar behaviour can be seen for both cases in which the yielding follows the mining front for all pillars except pillar 6 and, to some extent, pillar 11. Based on this it was decided to further analyse pillars 6 and 9 because they represent two general cases for a pillar that does not yield and one that yields as desired.

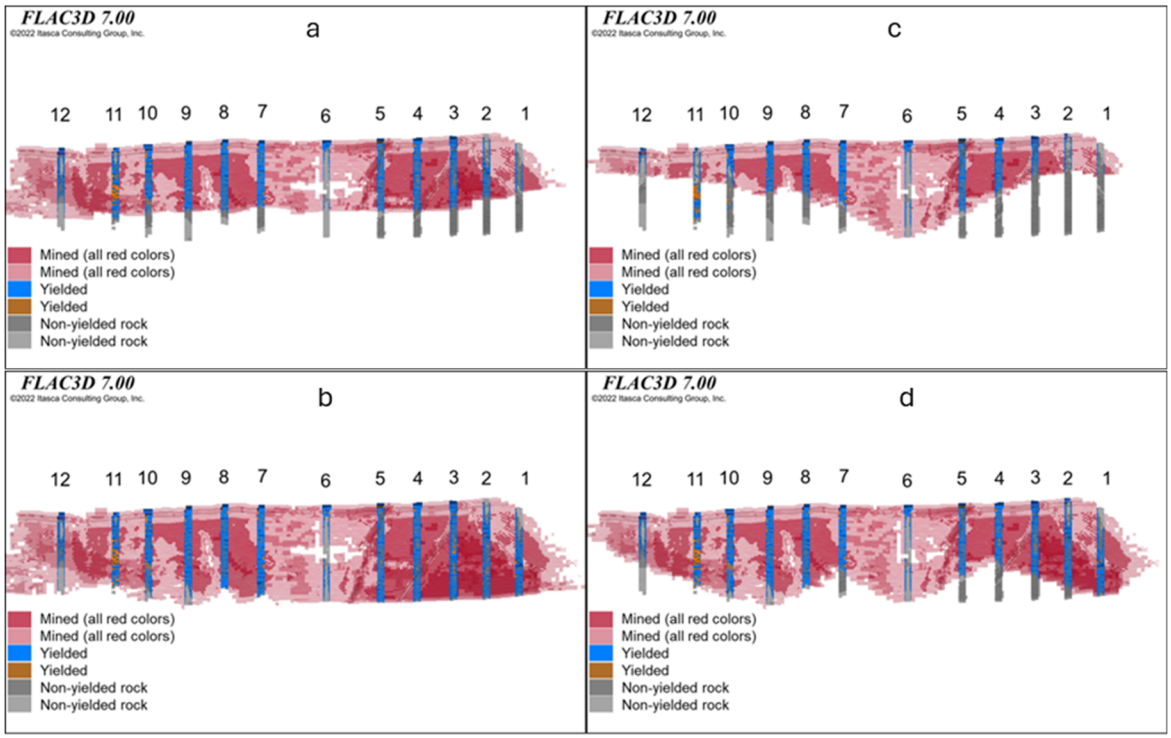

Figure 12 Yielding in the pillars where (a) and (b) show the base case for mining in 2035 and 2055 while (c) and (d) show equivalent years 2020 and 2039

In the initial stages of mining, results show that inside pillar 9 is a concentration of stresses located in the top of the pillar. A plausible reason for this is that since everything above the pillar is mined, the stresses from the footwall and hanging wall above the pillar will concentrate near the pillar top. Hence even if the top portion has yielded, an increase in confinement can still result in a significant load-bearing capacity and thus allow stress to transfer through this area. As mining advances, the mid-sections (in height) of the pillar also start to yield. In comparison to the top of the pillar, the mid-section of the pillar experiences a reduction in stress where the stress magnitudes inside are much closer to those in the surrounding rock (Figure 13). The abutment of the pillar does, however, remain highly stressed.

The orebody becomes thinner and more irregular towards depth in this area. Hence in the final mining stages the pillar does not yield for around three mining levels above the mining front. As result there is a high-stress area located at and above the mining front. A consequence of this is that any mining on this level would be close to a highly stressed pillar, with a larger potential for a brittle rather than ductile failure.

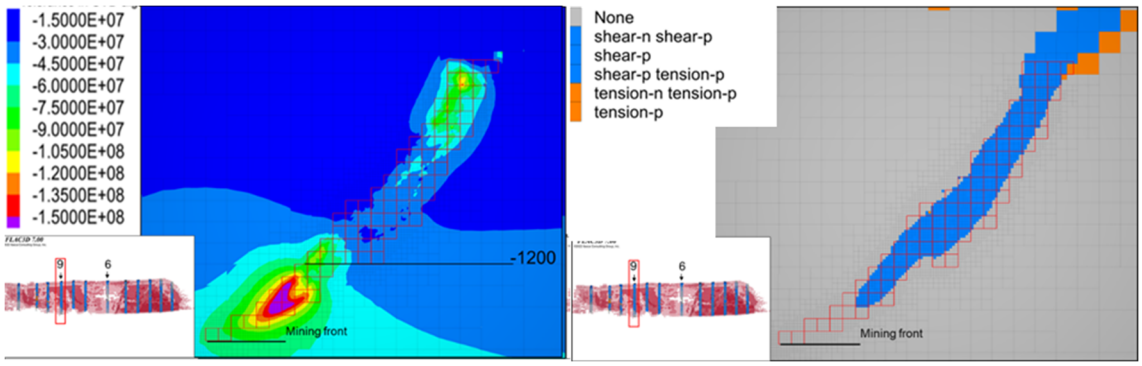

(a) (b)

Figure 13 (a) Major principal stress in pillar 9 for planned year 2055; (b) Rock mass yielding in pillar 9 for planned year 2055

In pillar 6 no, or very limited, yielding develops during the entire mining progress. This is even though the span between pillar 6 and the neighbouring pillars to the north and south is much larger than for the other pillars. There are a couple of possible causes for this behaviour. While the pillar has the same 60 m width along strike as the other pillars, the effective width of this pillar near the middle is much larger than 60 m after excavation. This is because ore dissipates in this area and removal of waste rock was not planned (Figure 14). The second possible contributor to the behaviour of pillar 6 is the local geology. Lenses of more competent porphyry rock are also located inside and around pillar 6 and influence the stress conditions. This indicates that the shape of the orebody and the geology are important factors in controlling the yielding of the pillars.

As a result, the pillar in this area will have a reverse hourglass shape with a wider part in the middle. This pillar geometry results in lower stress in the middle area compared to portions of the pillar above or below, simply because there is more area for the stress to be transferred through. Since large parts of the pillar do not yield it will remain heavily stressed, with an increased hazard for brittle failure (see Figure 15).

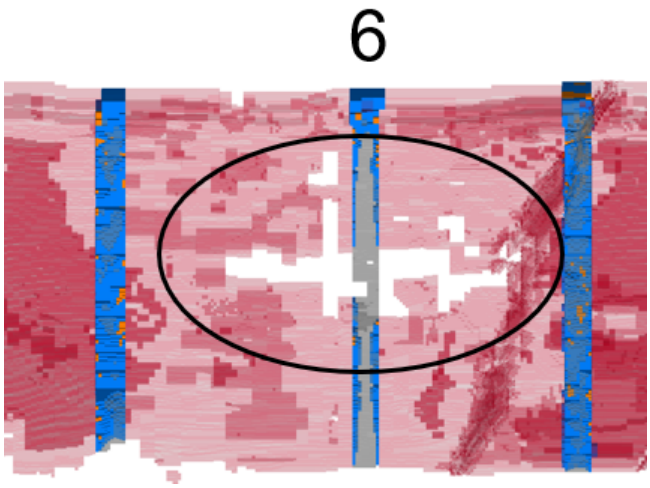

Figure 14 Zoomed in portion of pillar 6 with a longitudinal view looking west. The red colour shows what is mined while the white area inside the circle is not mined since it is either the unmined 1,022 m and 1,052 m levels in block 22 or porphyry rock (not ore)

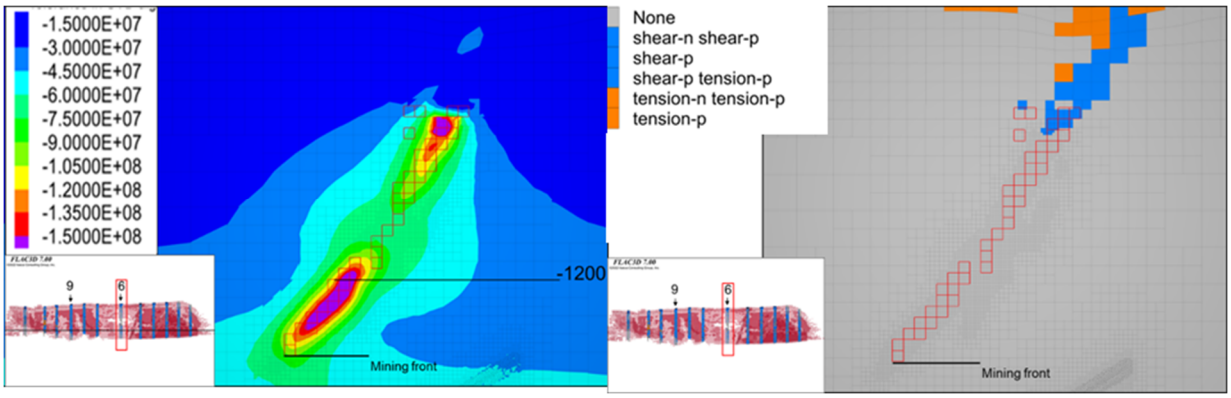

(a) (b)

Figure 15 (a) Major principal stress in pillar 6 in planned year 2055; (b) Rock mass yielding in pillar 6 in planned year 2055

6 Conclusion

The use of a chevron-shaped mining sequence results in both an overall decrease in released energy as well as reduced peaks of the available energy when compared to the base case mining sequence. For the chevron

case the energy is also generally spread over more production blocks compared to the base case, since the production is spread over a larger portion of the orebody in comparison to the base case.

The introduction of yielding pillars successfully reduces the available seismic energy for both the base and the chevron cases. When using yielding pillars, the pattern for the energy distributions in each production block per year is similar but the pillars reduce the magnitude of the energy. It is unclear if the underlying cause of this is the effect of pillars on stress and convergence, and/or the reduced mining tonnage caused by the pillars, and how much each factor is contributing.

The yielding in pillars is highly dependent on local geology and ore thickness, and not just the span between pillars. Findings shows that a thin (60 m along orebody strike) pillar placed in block 22 would not yield even with distances to the neighbouring pillars being around 450 m. However, this pillar widens extensively along the orebody strike in the middle due to a lack of ore at these mining levels. This unusual pillar shape likely contributes to the results, as well as the fact that part of the pillar is in porphyry rock with different properties. Further optimisation of pillar dimensions is required to ensure ductile yielding of the pillars.

There is a weak qualitative agreement between calculated released energy and seismicity in the mine. However, a quantitative agreement could not be established. The accuracy in relating potential seismic energy in the model to actual events in time and production block location can probably be improved with a more detailed mining sequence and a different way of calculating energy from the model. However, some events may still occur far away from the point of energy release if there are weak links in the overall system.

Acknowledgement

This project was initiated by, and part of, the MIGS IV Consortium, managed by HeadMining AB. The authors gratefully acknowledge LKAB for its financial support and permission to publish this paper.

References

Dahnér, C, Malmgren, L & Bošković, 2012, 'Transition from non-seismic mine to a seismically active mine: Kiirunavaara Mine', *Eurock 2012: Proceedings Rock Engineering and Technology for Sustainable Underground Construction,* International Society for Rock Mechanics, Lisbon.

du Plessis, M 2018, 'Manuel Rocha Medal recipient: the design and behaviour of crush pillars on the Merensky Reef', in Z Zhao, Y Zhou & J Shang (eds), *Proceedings of the 10th Asian Rock Mechanics Symposium (ARMS10), Singapore – The 2018 ISRM International Symposium*.

Ghazvinian, E, Garza-Cruz, T, Bouzeran, L, Fuenzalida, M, Cheng, Z, Cancino, C & Pierce, M 2020. 'Theory and implementation of the Itasca Constitutive Model for Advanced Strain Softening (IMASS)', *Proceedings of the Eighth International Conference and Exhibition on Mass Mining (MassMin 2020)*, University of Chile, Santiago, pp. 451–461.

Hedley, DGF 1992, *Rockburst Handbook for Ontario Hardrock Mines*, CANMET Special Report SP92-1E.

ITASCA 2022, *FLAC3D (Fast Lagrangian Analysis of Continua 3D)*, version 7, computer software, Itasca Consulting Group, Inc., Minneapolis.

Mortazavi, A & Brummer, RK 2000, *The Behaviour of Sill Pillars and Highly-Stressed Remnants*, report to CAMIRO Mining Division, Itasca Consulting Canada Inc., Sudbury.

Ortlepp, D 1983, 'Chapter 12: the mechanism and control of rockbursts', in S Budavari (ed.), *Rock Mechanics in Mining Practice*, The South African Institute of Mining and Metallurgy, Johannesburg.

Sandström, D 2003, *Analysis of the Virgin Stress State at the Kiirunavaara Mine*, licentiate thesis, Luleå University of Technology, Luleå.

Svartsjaern, M, Rentzelos, T, Shekhar, G, Swedberg, E, Boskovic, M & Hebert, Y 2022, 'Controlled reopening of the Kiirunavaara production block 22 after a 4.2 magnitude event', in Y Potvin (ed.), *Caving 2022: Proceedings of the Fifth International Conference on Block and Sublevel Caving*, Australian Centre for Geomechanics, Perth, pp. 685–698, https://doi.org/10.36487/ACG_repo/2205_47